

Regulators of Metastasis Modulate the Migratory Response to Cell Contact under Spatial Confinement

Daniel F. Milano,¹ Nicholas A. Ngai,³ Senthil K. Muthuswamy,^{3,4,*} and Anand R. Asthagiri^{1,2,*}

¹Department of Chemical Engineering and ²Department of Bioengineering, Northeastern University, Boston, Massachusetts; ³Princess Margaret Cancer Center, University of Toronto, Toronto, Ontario, Canada; and ⁴Beth Israel Deaconess Medical Centre, Harvard Medical School, Boston, Massachusetts

ABSTRACT The breast tumor microenvironment (TMEN) is a unique niche where protein fibers help to promote invasion and metastasis. Cells migrating along these fibers are constantly interacting with each other. How cells respond to these interactions has important implications. Cancer cells that circumnavigate or slide around other cells on protein fibers take a less tortuous path out of the primary tumor; conversely, cells that turn back upon encountering other cells invade less efficiently. The contact response of migrating cancer cells in a fibrillar TMEN is poorly understood. Here, using high-aspect ratio micropatterns as a model fibrillar platform, we show that metastatic cells overcome spatial constraints to slide effectively on narrow fiber-like dimensions, whereas nontransformed MCF-10A mammary epithelial cells require much wider micropatterns to achieve moderate levels of sliding. Downregulating the cell-cell adhesion protein, E-cadherin, enables MCF-10A cells to slide on narrower micropatterns; meanwhile, introducing exogenous E-cadherin in metastatic MDA-MB-231 cells increases the micropattern dimension at which they slide. We propose the characteristic fibrillar dimension (CFD) at which effective sliding is achieved as a metric of sliding ability under spatial confinement. Using this metric, we show that metastasis-promoting genetic perturbations enhance cell sliding and reduce CFD. Activation of ErbB2 combined with downregulation of the tumor suppressor and cell polarity regulator, PARD3, reduced the CFD, in agreement with their cooperative role in inducing metastasis *in vivo*. The CFD was further reduced by a combination of ErbB2 activation and transforming growth factor β stimulation, which is known to enhance invasive behavior. These findings demonstrate that sliding is a quantitative property and a decrease in CFD is an effective metric to understand how multiple genetic hits interact to change cell behavior in fibrillar environments. This quantitative framework sheds insights into how genetic perturbations conspire with fibrillar maturation in the TMEN to drive the invasive behavior of cancer cells.

INTRODUCTION

The tumor microenvironment (TMEN) is a dynamic site where cell movements and matrix remodeling are in flux. How tumor cells navigate this complex environment and disperse from the primary tumor is critically important for tumor growth and metastasis. Emerging work in the breast TMEN shows that metastatic breast cancer cells migrate along protein fibers (1,2). During breast cancer progression, tumor-associated fibroblasts reorganize the extracellular matrix and align collagen fibers perpendicular to the tumor-stromal boundary to facilitate invasion (3,4). These adhesive fibers, which can reach 1–8 μm in diameter (5–7), serve as guidance cues that direct cells away from the primary tumor (1). In fact,

the extent of fiber alignment at the tumor boundary has been correlated with invasion and been suggested as a prognostic indicator for advanced disease in breast cancer patients (8).

Within this fibrillar context, migrating cells are constantly interacting with each other. How these cell-cell interactions affect the migration of cancer cells has important implications for metastasis. Cancer cells that circumnavigate encounters with other cells will maintain their migratory path along protein fibers, thereby taking a less tortuous path out of the primary tumor. Alternatively, collisions with other cells may block or turn back cancer cells, thereby reducing the efficacy of invasion. How normal and cancer cells respond to cell-cell contact in a confined, fibrillar microenvironment and to what extent physical parameters, such as the fiber dimensions, influence the contact response and its dynamics are unclear.

Interactions between migrating cells have been studied in traditional two-dimensional (2D) cell culture substrates

Submitted November 12, 2015, and accepted for publication February 23, 2016.

*Correspondence: a.asthagiri@neu.edu or smuthusw@bidmc.harvard.edu

Editor: Stanislav Shvartsman.

<http://dx.doi.org/10.1016/j.bpj.2016.02.040>

© 2016 Biophysical Society

where the phenomenon of contact-inhibition of locomotion (CIL) was originally reported by Abercrombie and colleagues (9,10). CIL describes the process by which migrating cells retract away from cell-cell contact, repolarize, and migrate apart (11). In contrast, migrating cells that fail to retract upon contact and only moderately deviate from their original direction of movement exhibit a loss of CIL. To what extent similar modes of behavior occur in a fibrillar context remains unclear.

In addition, the molecular mechanisms that regulate cell-cell contact response in spatially constrained fibrillar environments are unknown. In a recent study the polarity protein PARD3 was found to mediate CIL in migrating neural crest cells in 2D culture and in vivo by promoting microtubule catastrophe at the contacting edge of interacting cells (12). We have previously identified PARD3 as a suppressor of breast cancer metastasis in vivo. We showed that the knockdown of PARD3 and induction of the proto-oncogene ErbB2 cooperatively induce metastasis in vivo by perturbing E-cadherin dynamics and compromising cell-cell cohesion without altering E-cadherin expression (13). Whether PARD3 regulates the contact response of migrating cells in a fibrillar context has yet to be determined.

To better understand the contact response of migrating cells in a fibrillar context, we conducted a quantitative analysis of migrating human breast epithelial cells on high aspect ratio micropatterned surfaces. Adhesive micropattern stripes provide a model platform to emulate a fiber-like one-dimensional microenvironment. Although adhesive stripes lack the three-dimensional (3D) topology and mechanical properties of in vivo fibers, cells confined on adhesive micropatterned stripes exhibit cell morphology, focal adhesion composition, and motile characteristics that are strikingly similar to counterparts migrating on 3D fibers in vivo (14,15). Furthermore, micropatterning provides a facile and robust method to investigate the effect of modulating spatial confinement by varying stripe width.

Here, we show that migrating metastatic breast cancer cells overcome the spatial constraints of narrow fibrillar-like micropatterns to circumnavigate or slide around collision partners during pairwise cell-cell interactions. On the other hand, nontransformed MCF-10A (10A) mammary epithelial cells predominantly reverse direction in response to cell-cell contact and slide only on the broadest micropatterns. Introducing metastasis-associated genetic perturbations reduces the fibrillar-like dimensions on which 10A cells slide, thereby quantitatively shifting 10A sliding behavior toward that of metastatic cells. By reducing the fibrillar dimensions at which slides are executed efficiently, our results suggest genetic perturbations work synergistically with fiber maturation in the TMEN to promote a more invasive sliding phenotype. Taken together, our results show that the contact response is a quantitative property and that the characteristic fibrillar-like dimension (CFD) at which cells exhibit efficient sliding is an effective metric

for quantifying relative invasive potential on fiber-like micropatterns. Using this metric, we show that molecular perturbations, such as the knockdown of E-cadherin, the knockdown of PARD3 in cooperation with ErbB2 induction, and transforming growth factor β (TGF- β) stimulation, contribute significantly to the acquisition of sliding ability.

MATERIALS AND METHODS

Micropatterning and surface preparation

Patterned surfaces were prepared via microcontact printing using poly(dimethylsiloxane) (PDMS) elastomeric stamps as described previously (16). Stamps were incubated with an equimolar solution of 10 $\mu\text{g}/\text{mL}$ fibronectin (Life Technologies, Carlsbad, CA) and 1.4 $\mu\text{g}/\text{mL}$ Alex Fluor 594 conjugated bovine serum albumin (BSA) (Invitrogen, Carlsbad, CA) dissolved in phosphate buffered saline (PBS) (Invitrogen). Stamps were rinsed with deionized water and blown dry with nitrogen. Stamps were left in contact with a plasma-treated (Harrick Plasma, Ithaca, NY), spin-coated PDMS surface for 10 min. Pluronic F127 (EMD Biosciences, San Diego, CA) diluted in PBS (0.02 vol%) was incubated with the surface for 15 min to prevent nonspecific cell adhesion and subsequently washed with PBS.

This study was conducted with 6–33 μm micropatterns to emulate the biophysical spatial confinement of in vivo 3D fibers with diameters (D) reported in the range of 1–8 μm (5–7). Because cells on 1–8 μm -wide 3D fibers can spread circumferentially around the fiber over a distance of $\pi D \sim 3\text{--}24 \mu\text{m}$, we sought to use micropatterns spanning these widths. Microcontact printing in our hands robustly yielded micropatterns with feature sizes above 5 μm . Thus, the lowest width of micropatterns used in this study was 6 μm , equivalent to a circumferential distance of a 2 μm -wide 3D fiber. At the upper limit, we extended to 33 μm -wide micropatterns to relax spatial confinement well beyond the diameter of individual MCF-10A cells.

Image acquisition and analysis

MCF-10A cells and MDA-MB-231 cells were seeded on patterned surfaces at a density of 2.0×10^4 cells/mL (Z2 Counter, Beckman Coulter, Danvers, MA) and incubated for 75 min and 150 min, respectively, to optimize the chance of two cells adhering on each patterned line. Phase contrast images were acquired for 21 h at 5-min intervals at $10\times$ magnification on a humidified microscope stage maintained at 37°C and 5% CO₂ (Axiovert 200M and Axiovision/Zen software, Carl Zeiss, Göttingen, Germany). At the conclusion of time-lapse imaging, the fluorescent micropattern was imaged at $20\times$ magnification (562 nm excitation, Texas Red filter). All frame-by-frame image analysis was performed in either Axiovision or Fiji (open-access). Pairwise collisions involving only two cells that distinctly form and break contact during the duration of the experiment were included in the analysis.

Cell culture

MCF-10A normal human mammary epithelial cells (ATCC, Manassas VA) were cultured as described previously (17). To induce epithelial-mesenchymal transition (EMT), cells were cultured for 12 days in growth medium supplemented with 20 ng/mL of recombinant human transforming growth factor beta-1 (Peprotech, Rocky Hill, NJ). MDA-MB-231 human metastatic breast cancer cells (ATCC) were cultured in high glucose Dulbecco's modified Eagle's medium (Invitrogen) supplemented with 10% fetal bovine serum (Invitrogen) and 1% penicillin/streptomycin (Invitrogen) under humidified conditions at 37°C and 5% CO₂. Cells were passaged regularly by dissociating 80% confluent monolayers with 0.05% trypsin-EDTA (Invitrogen) and reseeding at 1:8 dilution. BT549 human metastatic breast cancer cells (ATCC) were cultured in RPMI 1640 base medium (Invitrogen) supplemented with 10% fetal bovine serum (Invitrogen) and 1% penicillin,

streptomycin (Invitrogen). Cells were maintained in humidified conditions at 37°C and 5% CO₂ and passaged regularly by dissociating 80% confluent monolayers with 0.05% trypsin-EDTA (Invitrogen) and seeding cells in fresh growth medium at 1:3 dilution.

Knockdown of PARD3 expression

The shRNA constructs against human PARD3 were obtained from The RNA Consortium lentiviral shRNA library (Open Biosystems, Thermo Scientific, Waltham, MA). TRC clone ID No. shPar3-TRCN0000118134, from TRC-Hs1.0 (Human), targeting human PAR3 (locus: NM 019619.3) 3112–3132 bp sequence: 5'-CCGGGCCATCGACAAATCTTATGATCTCGAGATCATAAGATTTGTGCGATGGCTTTTTG-3' was used to generate pooled populations of 10A cells stably expressing the shRNA.

E-cadherin perturbations

shRNA were expressed using the pLKO.1 lentiviral vector system as described by The RNAi Consortium (TRC) protocols. shECAD: hairpin 5'-CCGGAGATTGCACCGTTCGACAAAGCTCGAGCTTTGTCGACCGGTGCAATCTTTTTG-3' targeting sequence AGATTGCACCGGTGCAAAAG derived from TRC clone TRCN0000237841. Following infection, 10A cells underwent puromycin (1 µg/mL) selection.

E-cadherin-GFP (ECAD-GFP) was obtained from Addgene (Cambridge, MA; plasmid 28009, deposited by Jennifer Stow). MDA-MB-231 cells were transfected using Lipofectamine 2000 (Life Technologies) according to manufacturer protocol. Stably transfected clones were expanded following G418 (400 µg/mL) selection.

ErbB2 induction

10A.B2 cells expressing the inducible ErbB2 construct and the incorporation of shRNA constructs targeting PARD3 and GFP were described previously (13,18). ErbB2 signaling was induced by treatment with 1 µM of AP1510 (Clontech, Mountain View, CA) for 48 h in 10A growth medium. Vehicle-only controls were performed by substituting AP1510 with 0.1 vol% ethanol.

Western blotting

E-cadherin and p42/44 MAP kinase were probed using 1:10,000 and 1:2000 dilution of primary antibodies (BD Biosciences, San Jose, CA and Cell Signaling Technologies, Danvers, MA, respectively) and 1:5000 dilution of HRP-conjugated secondary antibody (GE Healthcare Life Sciences, Pittsburgh, PA). Western blots were imaged by enhanced chemiluminescence (Thermo Scientific, Waltham, MA), captured by a charge-coupled device camera, and quantified by densitometry using Fiji (open-access).

Data analysis and statistics

Data analysis was conducted in MATLAB (The MathWorks, Natick, MA). Analysis of variance (ANOVA) and Tukey's post hoc statistical analysis were conducted in SPSS software (IBM, Armonk, NY).

RESULTS

Metastatic breast cancer cells exhibit efficient sliding behavior in fiber-like dimensions

To better understand the response of migrating cells to cell-cell contact in a fibrillar-like spatially constrained

microenvironment, we used microcontact printing to fabricate micropatterned lines of fibronectin on a PDMS spin-coated glass surface. A trace amount of BSA-Cy3 was used to confirm directly that the micropattern dimension matched the corresponding feature size of the PDMS stamp (Fig. 1 A). Cells were confined to the adhesive micropatterns by blocking nonpatterned areas with Pluronic F127, a block copolymer.

Using time-lapse microscopy, we examined how individually migrating nontransformed mammary epithelial MCF-10A (10A) cells and metastatic MDA-MB-231 (231) breast cancer cells respond to homotypic interactions with a neighboring cell in this model fibrillar environment. We analyzed collisions involving two individually migrating cells that initiated and broke cell-cell contact within the observation period. Initiation and cessation of cell-cell contact was determined by time-lapse phase contrast microscopy and recording the time at which membrane protrusions of two cells first contact and the time at which a cell pair disengages and no longer has physical contact, respectively. Another outcome is also possible: two cells could come in contact and fail to come apart within the duration of observation. However, it is difficult to discern whether the pair of cells had indeed formed a stable adhesion or whether the pair would have come apart if observed for a longer time. We therefore initially focused on cell pairs that interact and come apart during observation and returned later to examine the possibility of a stable adhesion (as described below).

On 24 µm-wide micropatterns, migrating 10A cells that collide predominantly come apart by repolarizing and reversing direction. This event was classified as a contact-initiated reversal (Fig. 1 B; see Movie S1 in the Supporting Material). Occasionally, one cell circumnavigated a neighboring cell, thereby maintaining its direction of migration. This response was categorized as a contact-initiated slide (Fig. 1 C; see Movie S2). The terms reversal and slide portray the two collision responses in morphological terms and are not meant to suggest underlying biophysical mechanisms. For example, a reversal in direction is certainly not an elastic interaction. In contrast to the contact response of 10A cells, 231 cells exhibited contact-initiated sliding more frequently. To quantify this response, we determined the fraction of observed collisions that resulted in cells coming apart through a slide versus reversal response. Although only 7.2% of collisions between 10A cells resulted in sliding (with the remaining 92.8% resulting in a reversal), metastatic 231 cells exhibited a slide response in ~52% of the collisions ($p < 0.05$) (Fig. 1 D).

We next investigated if the availability of free surface area contributed to the ability of cells to slide by varying the width of the micropattern lines. Cells were plated on narrow micropatterns of 6 µm, approximating the dimensions of 1–8 µm fibers observed *in vivo* (5–7), up to wide 33 µm micropatterns, nearly the width of two cell diameters (see

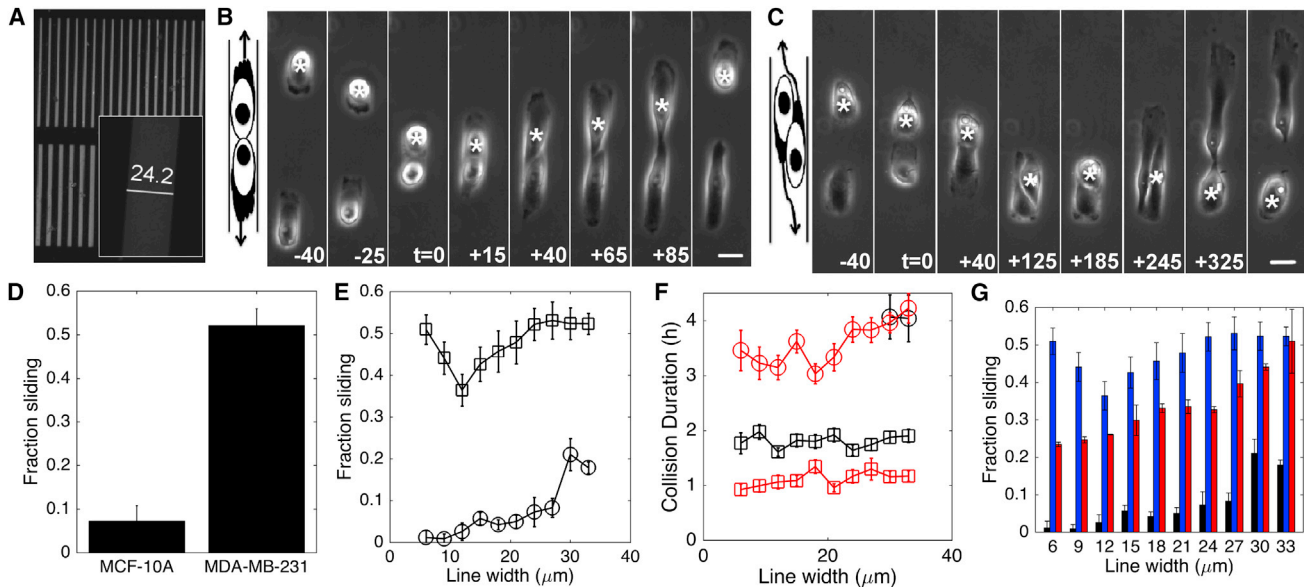


FIGURE 1 Cells respond to collisions by reversing or maintaining their migratory path to slide around the partner. (A) Fibronectin lines of varying width are patterned onto an elastomeric surface and measured by copatterning Cy3-tagged BSA (*inset*). Representative time points of MCF-10A cells undergoing reversal (B) and slide (C) collision. Asterisk marks the same cell across each time series. Time $t = 0$ corresponds to the start of the interaction. Scale bars, 20 μm . (D) The fraction of collisions that resulted in a sliding response is reported for 10A and MDA-MB-231 cells migrating on 24- μm lines. (E) Fraction sliding for 10A (*circles*) and 231 (*squares*) as a function of pattern line width. (F) Reversal (*squares*) and sliding (*circles*) collision dynamics measured as a function of line width for 231 (*red*) and 10A (*black*) cells. Sliding dynamics for 10A cells (*black circles*) were measured only on 30 and 33 μm wide lines where a sufficient number of events for statistical analysis were observed. (G) Fraction sliding as a function of pattern line width for BT-549 (*red bars*), and for comparison, data for 10A (*black bars*) and 231 (*blue bars*) is replotted from Fig. 1 E. Error bars denote SE.

Materials and Methods for a further description of micropattern widths). On all of the line widths, metastatic 231 cells continued to undergo more frequent sliding collisions than nontransformed 10A cells (Fig. 1 E). Except for a modest reduction at 12 μm -wide stripes, the propensity of sliding among 231 cells is maintained at $\sim 50\%$ across all micropattern dimensions. In contrast, 10A cells exhibit a maximum sliding frequency of 20% at the broadest line widths (30–33 μm), and the frequency of slides drops sharply as the width of the micropattern is reduced. On the narrowest micropatterns (6 and 9 μm), only two of the 205 observed collisions resulted in a sliding response. Taken together, these results demonstrate that metastatic 231 cells exhibit greater ability to slide than nontransformed 10A cells and that the spatial constraints of a narrow, fibrillar-like micropattern significantly suppresses the sliding of nontransformed cells but not metastatic 231 cells.

We next investigated whether the differential responses to cell-cell collisions is associated with underlying differences in single-cell migration behavior. A possibility is that cells that are inherently more persistent in their migration may maintain their direction of movement even upon encountering other cells. To test this possibility, we quantified the persistence of individually migrating 10A and 231 cells on narrow (6 μm) and moderately (18 μm) wide micropatterns. Our quantification showed that 10A cells maintained their direction of movement on average for 28 min compared to a persistence time of 16 min for 231 cells. Thus, higher

persistence of single-cell migration does not correlate with better sliding ability. Similar analysis of single-cell migration speeds reveals no correlation to cell sliding behavior (Supporting Material). These results demonstrate that the response of migrating cells to cell-cell collisions is decoupled from their single-cell migration behavior.

To better characterize the collisions, we quantified the dynamics of reversal and slide responses. For each collision, we recorded the duration from when a pair of cells first comes in contact to the point when the cells come apart. In general, sliding collisions took significantly longer to execute than reversal collisions. MDA-MB-231 cells took an average of 3.6 h to complete a slide. On micropattern widths of 30–33 μm , 10A cells executed a sufficient number of slides to gather statistically meaningful data on the dynamics. On these patterns, 10A cells took an average of 4.1 h to execute a slide, a duration on par with 231 cells. For reversal collisions, 231 cells executed them faster than 10A cells ($p < 0.05$) (Fig. 1 F). On average, 10A cells took 1.8 h to complete a reversal response after initial contact, whereas 231 cells required only 1.1 h. Taken together, this characterization of collision dynamics reveals that contact-initiated sliding is a kinetically slower process than the touch-and-retract response of a contact-initiated reversal. The slower dynamics of a slide is consistent with the fact that while both reversing and sliding involve cells forming adhesions and ultimately breaking those adhesions to come apart, executing a slide is likely to involve

additional cellular processes by which a cell migrates around a neighbor while maintaining cell-cell contact.

Quantifying the dynamics of reversal and slide events provides a foundation to assess systematically the occurrence of stable adhesions. We reasoned that if a pair of cells remained together longer than the characteristic time needed to separate (t_{sep}), this pair may be scored as having formed a stable adhesion. We quantified $t_{\text{sep}} = 5.8$ h as the time it takes for 95% of pairwise cell-cell interactions to come apart in a reversal or slide. Using this criterion, we reanalyzed three independent experiments, consisting of 952 pairwise collisions. Only 26 pairs of 10A cells initiated contact and remained together for longer than t_{sep} , amounting to 2.7% of all pairwise collisions resulting in stable adhesion. Thus, the dominant outcome of pairwise cell interactions is a breakup of the pair, either by a slide or a reversal.

Finally, to confirm that the significant increase in sliding frequency observed in 231 cells was not unique to this cancer cell line, we examined the contact response of another metastatic breast cancer cell line, BT-549 cells. Similar to 231 cells, BT-549 cells exhibit a significantly higher ability to slide than nontransformed 10A cells across all micropatterned line widths (Fig. 1 G). On the narrowest micropattern widths, ~25% of BT-549 and ~50% of 231 cell collisions result in a sliding response; in contrast, <5% of 10A collisions generate a slide under these conditions that mimic fibrillar-like dimensions.

E-cadherin expression regulates sliding behavior

The loss of E-cadherin expression is correlated with breast cancer progression (19,20). To determine whether downregulation of E-cadherin expression enhances sliding behavior in a fibrillar-like microenvironment, we knocked down the expression of E-cadherin by transducing 10A cells with a lentivirus encoding shRNA targeting E-cadherin. As a negative control, cells were infected with empty vector lentivirus. Knockdown of E-cadherin was confirmed by Western blot, and densitometry analysis showed that the short hairpin construct reduced E-cadherin expression to 40% of the level expressed in control 10A-pLKO cells (Fig. 2 A). Analysis of cell-cell collisions showed that diminishing E-cadherin expression enhances the likelihood of sliding (Fig. 2 B), particularly at line widths $>18 \mu\text{m}$.

Next, we asked if upregulating E-cadherin expression in 231 cells is sufficient to inhibit cell sliding. We generated 231 cells expressing E-cadherin by stable transfection and confirmed expression of exogenous E-cadherin by Western blot (Fig. 2 A). The level of exogenous E-cadherin expression is ~10% of the endogenous E-cadherin level in 10A cells. Meanwhile, as observed in other reports (19,21), parental 231 cells lack detectable levels of E-cadherin.

Introducing E-cadherin expression in 231 cells significantly reduces the frequency of sliding collisions across the full range of line widths (Fig. 2 B). Furthermore, the de-

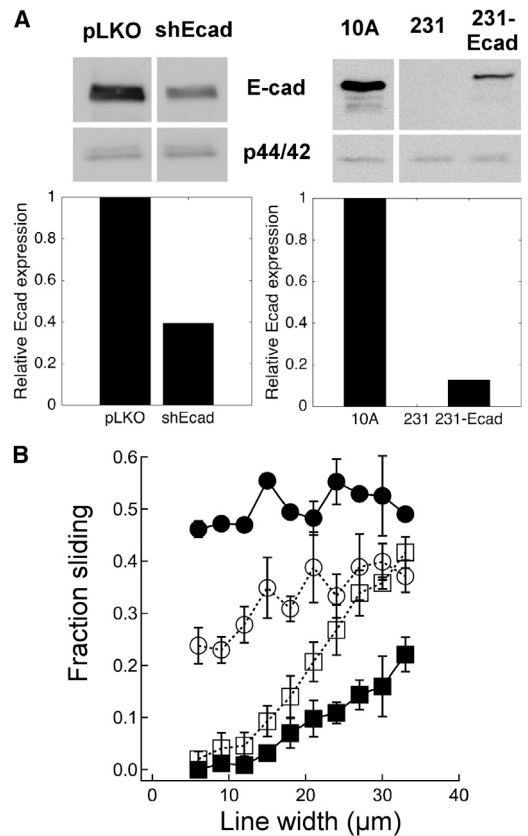


FIGURE 2 E-cadherin expression modulates sliding ability. (A) E-cadherin knockdown was confirmed by Western blot in MCF-10A cells expressing shRNA hairpin targeting E-cadherin (shEcad) or its empty-vector control (pLKO). E-cadherin expression in MDA-MB-231 cells stably transfected with E-cadherin-GFP (231-Ecad) is compared to 231 and 10A cells. Equal loading assessed using anti-p44/42 MAP kinase antibody, and relative E-cadherin protein expression quantified by densitometry. (B) Fraction sliding as a function of line width for 10A-shEcad (open squares) vs. 10A-pLKO cells (solid squares) and 231-Ecad (open circles) vs. parental 231 cells (solid circles). Error bars denote SE.

gree of reduction in sliding is greater where the cells are more spatially constrained. Thus, on $6 \mu\text{m}$ micropatterns, the likelihood of sliding diminished by twofold: 231-Ecad cells execute a slide in 25% of collisions compared to ~50% sliding among the parental 231 cells. Meanwhile, on broad $33 \mu\text{m}$ micropatterns, the fraction sliding reduces from ~50% in parental 231 cells to ~38% in 231-Ecad cells. Taken together, these results demonstrate that overexpressing E-cadherin mitigates the ability of 231 cells to slide and imparts a greater sensitivity to micropattern dimensions when executing slide responses.

PARD3 and ErbB2 cooperatively regulate cell sliding behavior

Recently, Moore et al. (12) found the polarity protein PARD3 regulates contact response behavior in neural crest cells by promoting microtubule catastrophe and inducing

repolarization at the cell-cell interface. We previously identified PARD3 as a suppressor of metastasis in breast cancer by showing the loss of PARD3 cooperates with the activation of the proto-oncogene ErbB2 to induce metastasis *in vivo* (13). Thus, we investigated if PARD3 loss and ErbB2 activation, either each alone or in cooperation, affect the contact response of 10A cells on fiber-like micropatterns.

MCF-10A cells were engineered with an inducible ErbB2 construct (10A.B2) that can be activated with the addition of a synthetic, small molecule dimerizer (AP1510), as previously described (18). To the 10A.B2 cells, we introduced short hairpin targeting either PARD3 (10A.B2-shPAR3) or GFP (10A.B2-shGFP) as a negative control (13).

Knockdown of PARD3 alone, without the induction of ErbB2, had no effect on cell sliding (Fig. 3 A). The sliding behaviors of 10A.B2-shGFP and 10A.B2-shPAR3 cells are

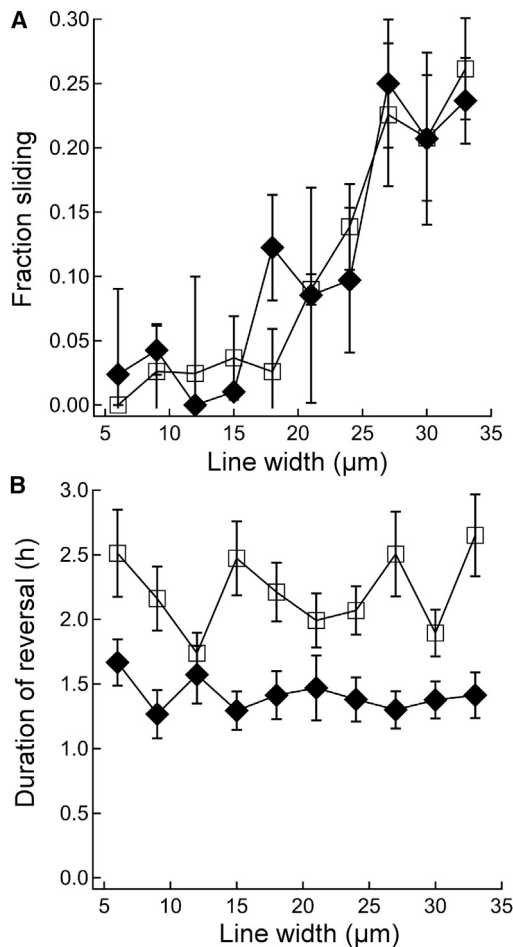


FIGURE 3 Knockdown of PARD3 alters collision dynamics without affecting the likelihood of sliding. (A) Fraction of collisions exhibiting sliding behavior in PARD3 knockdown cells (solid diamonds) in comparison to control cells (open squares) as a function of micropatterned line width. Error bars denote SE. $p > 0.05$ by ANOVA. (B) Contact duration of reversal collisions as a function of line width for PARD3 knockdown (solid diamonds) and control (open squares) cells. Error bars denote SE. $p < 0.05$ by ANOVA.

indistinguishable with fewer than 10% of collisions resulting in slides for micropatterns with a width $< 24 \mu\text{m}$. Only on the widest micropatterns (27–33 μm), the fraction sliding increases to ~ 20 –25% in a manner similar to the behavior of parental 10A cells (Fig. 1 E). The predominantly reversal response of cells with reduced PARD3 expression correlates with our prior observation that the loss of PARD3 alone is insufficient to induce metastasis *in vivo* (13).

Because PARD3 regulates E-cadherin dynamics and maturation (13), we asked whether the reduction in PARD3 expression has an effect on the dynamics of cell-cell collisions. For control cells expressing normal levels of PARD3, the lifetime of contact-initiated reversal fluctuates between 2 and 2.5 h with no apparent dependence on micropattern dimensions (Fig. 3 B). Meanwhile, downregulation of PARD3 reduces the lifetime of a reversal collision to ~ 1.5 h, which is ~ 50 –75% quicker than the duration of reversals observed in control 10A.B2-shGFP cells. These findings show that although loss of PARD3 is insufficient to induce sliding, PARD3 regulates the speed with which reversal collisions are executed, consistent with its role in regulating E-cadherin dynamics and maturation.

We next asked to what extent ErbB2 acts cooperatively with PARD3 to affect the sliding behavior of 10A cells. Activating ErbB2 alone using AP1510 in 10A.B2-shGFP cells had no effect on sliding in comparison to vehicle-treated 10A.B2-shGFP or 10A.B2-shPAR3 cells (Fig. 4). Thus, neither the activation of ErbB2 alone nor the

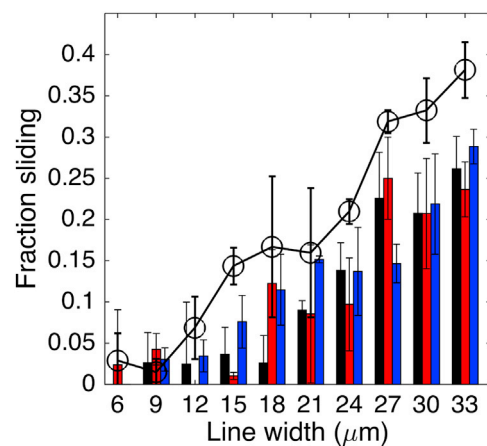


FIGURE 4 Knockdown of PARD3 and induction of ErbB2 cooperatively enhance sliding behavior. MCF-10A cells expressing an inducible ErbB2 construct (10A.B2) were engineered to coexpress either shRNA hairpin targeting PARD3 (10A.B2-shPAR3) or control shRNA hairpin targeting GFP (10A.B2-shGFP). The sliding behavior was quantified for 10A.B2-shGFP treated with vehicle (black bars) or AP1510 to induce ErbB2 (blue bars) and for 10A.B2-shPAR3 cells treated with vehicle (red bars). The vehicle-treated 10A.B2-shGFP (black bars) and 10A.B2-shPAR3 cells (red bars) are replotted from Fig. 3 A for comparison. The combined effect of PARD3 and ErbB2 was measured in 10A.B2-shPAR3 cells treated with AP1510 (black line). Error bars denote SE. ANOVA shows that only the 10A.B2-shPAR3 + AP1510 (black line) is statistically distinguishable from the other three cases ($p < 0.001$).

reduction of PARD3 expression alone induces sliding. Notably, activating ErbB2 using AP1510 in the background of PARD3 knockdown (Fig. 4, black line) enhances sliding frequency above control cells and above individual manipulation of PARD3 or ErbB2, particularly at line widths above 12 μm . These results demonstrate that PARD3 and ErbB2 cooperatively promote the acquisition of sliding behavior, consistent with their synergistic role in inducing metastasis in vivo.

Metastasis-promoting genetic perturbations enable sliding on narrower micropatterns

During cancer progression, collagen fibers become more aligned, and these aligned fibers provide broader pathways for cell invasion. An intriguing question is whether genetic perturbations that promote metastasis reduce the breadth of collagen tracks needed for invasive behavior. To probe this question, we determined the effect of metastasis-promoting genetic perturbations on the CFD at which cells achieve efficient sliding. Based on our measurements of sliding, we used a simple linear model to describe the dependence of sliding on micropattern width and quantified a value for the CFD at which cells achieve an intermediate level of sliding, i.e., 25% of collisions result in a slide (see Fig. S1). Although highly metastatic 231 and BT-549 cells achieve intermediate sliding efficiency on micropatterns smaller than 10 μm , nontransformed cells are at the other end of the spectrum, requiring micropatterns wider than 33 μm . Meanwhile, genetic perturbations that promote metastasis, such as the knockdown of E-cadherin or the combined perturbation of ErbB2 and PARD3, enable sliding at narrower micropattern widths than unperturbed 10A cells (Fig. 5 A). These findings demonstrate that genetic perturbations associated with metastasis quantitatively reduce the fibrillar dimensions at which cells are able to execute sliding behavior and that the CFD to achieve intermediate sliding efficiency provides a metric for quantitatively comparing metastatic potential.

To test further the suitability of CFD as a quantitative metric of the capacity to slide, we investigated the effect of adding a third perturbation, TGF- β , in combination with manipulating ErbB2 and PARD3. The sliding behavior was quantified for 10A.B2-shGFP and 10A.B2-shPAR3 cells in the presence of AP1510 or vehicle control and with or without treatment with 20 ng/mL TGF- β (see Fig. S2). Treatment with TGF- β increased the frequency of sliding when compared to untreated counterparts (Fig. S2, compare bars and lines of the same color). Joint activation of TGF- β and ErbB2 stimulated greater sliding than either stimulation alone, consistent with the cooperativity of TGF- β and ErbB2 in promoting invasion of MCF-10A cells (22). Finally, the three-way perturbation stimulated the greatest level of sliding in comparison to all two-way and one-way perturbations.

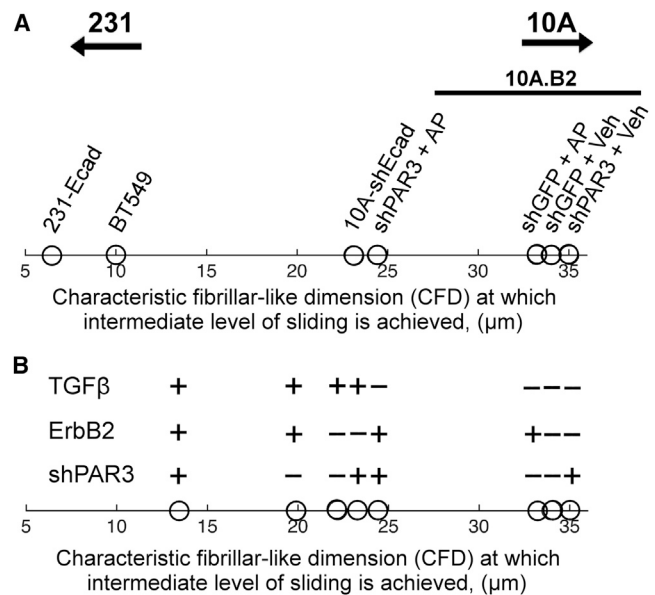


FIGURE 5 Quantifying contact response due to combinations of genetic perturbations. (A) The CFD at which cells exhibit moderate sliding efficiency was quantified. Arrows indicate that the CFD for MCF-10A cells and MDA-MB-231 cells is $>35 \mu\text{m}$ and $<5 \mu\text{m}$, respectively. Knockdown of E-cadherin (10A-shEcad) reduces the CFD, whereas the expression of exogenous E-cadherin in 231 cells (231-Ecad) increases CFD. Downregulation of PARD3 and activation of ErbB2 (10A.B2-shPAR3 + AP) reduces the CFD, but either perturbation alone has no effect on CFD relative to the control (10A.B2-shGFP + Veh). (B) The effect of TGF- β treatment along with perturbations in PARD3 and ErbB2 on the CFD. Treatment of cells with TGF- β reduces the value of CFD compared to untreated cells. Additionally, TGF- β treatment has a superimposable effect on reducing the CFD when combined with single and/or multiple genetic perturbations.

The CFD to achieve intermediate sliding efficiency was quantified for all combinations of molecular perturbations (Fig. 5 B). The values of CFD revealed a quantitative and progressive shift in the capacity of cells to slide in response to multiple perturbations. Single perturbations of downregulating PARD3 or inducing ErbB2 did not significantly differ from the control case: the value of CFD for these cells was $\sim 32\text{--}35 \mu\text{m}$. In contrast, exposure to TGF- β alone without perturbing PARD3 or ErbB2 reduced CFD to 23 μm , a value comparable to that of the double PARD3/ErbB2 perturbation. Thus, EMT-inducing TGF- β treatment was quantitatively equivalent to the combined PARD3/ErbB2 perturbation, which we have shown previously stimulates no overt EMT (13).

In addition, the three-way perturbation reduced the micropattern width needed for sliding to $\sim 13 \mu\text{m}$ (Fig. 5 B), near the level observed for BT549 cells (Fig. 5 A). Thus, EMT-inducing TGF- β treatment and EMT-free PARD3/ErbB2 perturbation have a cumulative effect on sliding behavior that is greater than each perturbation alone. The cumulative effect suggests that EMT-associated and EMT-independent pathways regulate sliding behavior through distinct mechanisms that are superimposable. Taken

together, these results demonstrate that the micropattern width at which cells achieve intermediate efficiency in sliding (CFD) provides an effective, quantitative metric to compare metastatic potential mediated by the accrual of multiple molecular perturbations.

DISCUSSION

Using high aspect ratio micropatterns as a fibrillar model, we show that migrating breast cancer cells overcome fiber-like spatial constraints and migrate around cells with which they come in contact. In fact, the disparity in contact-initiated sliding between normal and cancer cells is most striking under the spatial constraints of a fibrillar microenvironment. On 6–9 μm wide micropatterns that approximate the ~1–8 μm collagen fibers observed in the *in vivo* TMEN (5–7), 231 and BT-549 cells are 50- and 25-fold, respectively, more proficient at sliding past a collision partner than nontransformed 10A cells. The order-of-magnitude disparity in contact-initiated sliding between normal and cancer cells is revealed under fiber-like spatial constraints but is masked on wider micropatterns (27–33 μm) where 25% of 10A cell collisions result in a slide and where cancer cells are only ~twofold better at sliding. Thus, fiber-like spatial constraints significantly suppress the ability of normal cells to slide, whereas cancer cells override this constraint and slide by neighboring cells.

The contact responses of migrating normal and cancer cells in a fibrillar context have some similarities and distinctions to the CIL behavior reported in classical 2D culture formats (9,10) and *in vivo* in zebrafish and *Xenopus* (23). In 2D, individually migrating, contact-inhibited cells retract membrane protrusions from cell-cell contact sites and repolarize to migrate away from their collision partner. Meanwhile, cells that have lost CIL maintain membrane protrusive activity in the contact zone and migrate with slight deflection in their trajectory (11,24). Within the spatially confined context of a fibrillar-like environment, we show that the CIL-like repulsion behavior results in contact-initiated reversal, whereas cells that have the ability to maintain their direction of migration exhibit a slide response. A key distinction, however, is that in 2D analysis, cancer cells exhibit CIL when encountering other cancer cells in a homotypic interaction; only when engaged in a heterotypic interaction with fibroblasts or endothelial cells, cancer cells exhibit a loss-of-CIL phenotype (9,24,25). Our results show that in a fibrillar context, homotypic engagement between breast cancer cells results in sliding behavior, revealing that the contact response of migrating cells is highly dependent on the microenvironmental context.

We show that the transition from reversal to slide behaviors in a fibrillar context is a progressive, quantitative process. We propose and demonstrate the use of a metric to quantify contact response, namely the CFD above which cells execute sliding behavior with moderate efficiency.

Cells with smaller values of CFD are able to overcome the spatial constraints of narrower fibrillar-like dimensions to execute sliding collisions with moderate efficiency. Thus, smaller values of CFD correspond to greater sliding ability and consequently a more metastatic phenotype. The measured values of CFD reveal a spectrum of contact response behavior, with the highly metastatic 231 cells in the low end and 10A at the high end and cells with cancer-promoting molecular signals, such as E-cadherin, PARD3, ErbB2, and TGF- β in the middle.

Quantifying contact response behavior using a platform that spans a range of fibrillar-like dimensions provides insight into the role of overt EMT in acquisition of an invasive phenotype. We find that molecular perturbations that do not induce overt EMT, such as the downregulation of E-cadherin and the joint induction of ErbB2 alongside downregulation of PARD3, reduce the CFD to the same degree as treatment with EMT-inducing TGF- β (Fig. 5). In fact, our measurements show that these perturbations have a superimposable effect on the frequency of sliding behavior. Thus, combining TGF- β treatment with the PARD3 downregulation/ErbB2 induction has a cumulative effect greater than either perturbation alone (Fig. 5 B).

In addition to revealing the equipotency and additive effect of genetic perturbations, our approach captures synergies among genetic perturbations that individually have no impact on promoting sliding frequency. Reducing PARD3 expression cooperates with the induction of ErbB2 to enhance cell sliding, whereas neither the loss of PARD3 nor the induction of ErbB2 alone is sufficient to induce cell sliding on our platform. This cooperativity of ErbB2 and PARD3 is in agreement with our prior work showing that the loss of PARD3 cooperates with the induction of ErbB2 signaling to promote metastasis *in vivo* (13). Meanwhile, in neural crest cells, it has been reported that PARD3 alone regulates CIL. Downregulation of PARD3 in these cells blocks microtubule catastrophe and induces loss of CIL (12). This difference in the role of PARD3 may be linked to the cell context studied. Although our study focuses on the role of PARD3 in nontransformed mammary epithelial cells, neural crest cells are mesenchymal and are a useful model of cells that have undergone EMT. Furthermore, our results examine the role of PARD3 in fiber-like microenvironments.

Although downregulating PARD3 alone does not affect the likelihood of cell sliding, our data show that PARD3 regulates the dynamics of cell-cell collisions. Reducing PARD3 expression shortens the time that cells interact with each other before retracting and reversing direction. This effect on cell-cell interaction dynamics is consistent with our prior observation that the loss of PARD3 diminishes E-cadherin maturation and increases the mobile fraction of E-cadherin at cell-cell junctions without affecting E-cadherin expression level (13). Loss of PARD3 affects E-cadherin dynamics by elevating Tiam1-mediated Rac1 activation, causing uncontrolled Arp2/3 activity and actin dynamics (13). Thus,

by enhancing E-cadherin dynamics at cell-cell adhesions, PARD3 regulates the duration of cell-cell interactions. Although this PARD3-mediated regulation of collision dynamics does not by itself translate into an effect on cell sliding behavior, it cooperates with ErbB2 to enable cell sliding.

The role of E-cadherin in cancer progression and metastasis is complex and likely context-dependent. Elevated E-cadherin expression was observed during collective invasion of breast cancer cells (26). In collective movement, E-cadherin expression may help support intercellular adhesion. Meanwhile, the data presented here show that the loss of E-cadherin expression promotes cell sliding in the context of interactions between two individually migrating cells. Thus, differences in context, collective versus noncollective movement, may be part of the reason for the distinct roles of E-cadherin in mediating invasive behavior. Additionally, our data show that while loss of E-cadherin promotes sliding, E-cadherin downregulation is not essential. The loss of PARD3 together with activation of ErbB2 promotes cell sliding and metastasis without altering E-cadherin expression (13). Taken together, our data and those presented by Cheung et. al. suggest the role of E-cadherin expression in metastatic disease progression depends on the context (e.g., collective movement) and on whether other molecular perturbations have been acquired to circumvent the need to modulate E-cadherin level (e.g., ErbB2/PARD3). This context-dependent role of E-cadherin underscores the significance of our finding that the acquisition of cell sliding behavior is a quantitative property. Many different pathways exist for going up and down the quantitative CFD scale of sliding behavior. In some contexts, it could be a reduction in E-cadherin; in other cases, E-cadherin levels may be unaffected or even increase, whereas other pathways (e.g., PARD3/ErbB2) are tuned to enable cell sliding. Thus, the CFD provides a metric for directly comparing the relative strength of different molecular perturbations and for identifying equivalent combinations of molecular pathways for achieving the same quantitative level of sliding.

Finally, because the CFD has a direct physical interpretation, it provides insight into the interplay between cancer-promoting genetic perturbations and the evolving fibrillar organization of the TMEN. The CFD is a spatial dimension above which cells are proficient in sliding. We find that cancer-promoting genetic perturbations reduce the fibrillar width needed to support sliding behavior, thereby lowering the measured value of CFD. Meanwhile, the value of CFD also represents the extent to which fibrillar dimensions must grow to capacitate sliding behavior. As cancers develop, fiber dimensions increase as collagen fibrils in the TMEN are cross-linked and become more aligned (4,7,27). Early tumors with minimal fibrillar composition have better prognosis than late-stage tumors with denser, more aligned fibers. In fact, a tumor-associated collagen

signature that scores the density and extent of alignment of collagen has been proposed as a prognostic indicator of breast cancer (8). Thus, our work provides a quantitative framework to understand how the evolving fibrillar TMEN works synergistically with multiple genetic perturbations to progressively promote sliding behavior, a phenotype strongly correlated with metastatic potential in vivo.

SUPPORTING MATERIAL

Supporting Materials and Methods, two figures, and two movies are available at [http://www.biophysj.org/biophysj/supplemental/S0006-3495\(16\)30113-8](http://www.biophysj.org/biophysj/supplemental/S0006-3495(16)30113-8).

AUTHOR CONTRIBUTIONS

D.F.M., S.K.M., and A.R.A. conceived and designed the experiments. D.F.M. and N.A.S. performed the experiments. D.F.M. and A.R.A. analyzed the results and wrote the article. All authors edited and commented on the manuscript.

ACKNOWLEDGMENTS

We thank the members of the Asthagiri group for helpful discussions and the Kostas Nanoscale Research Center at Northeastern University for providing infrastructure for microfabrication.

This work was supported by the National Institutes of Health grants R01CA138899 to A.R.A. and R01CA098830 to S.K.M. and the Era of Hope Scholar Award from the Department of Defense (DOD) Breast Cancer Research Program to S.K.M.

REFERENCES

1. Wang, W., J. B. Wyckoff, ..., J. S. Condeelis. 2002. Single cell behavior in metastatic primary mammary tumors correlated with gene expression patterns revealed by molecular profiling. *Cancer Res.* 62:6278–6288.
2. Roussos, E. T. E., M. Balsamo, ..., J. S. J. Condeelis. 2011. Mena invasive (MenaINV) promotes multicellular streaming motility and transendothelial migration in a mouse model of breast cancer. *J. Cell Sci.* 124:2120–2131.
3. Theveneau, E., and R. Mayor. 2010. Integrating chemotaxis and contact-inhibition during collective cell migration: small GTPases at work. *Small GTPases.* 1:113–117.
4. Provenzano, P. P., K. W. Eliceiri, ..., P. J. Keely. 2006. Collagen reorganization at the tumor-stromal interface facilitates local invasion. *BMC Med.* 4:38.
5. Saidi, I. S. I., S. L. S. Jacques, and F. K. F. Tittel. 1995. Mie and Rayleigh modeling of visible-light scattering in neonatal skin. *Appl. Opt.* 34:7410–7418.
6. Sidani, M., J. Wyckoff, ..., J. Condeelis. 2006. Probing the microenvironment of mammary tumors using multiphoton microscopy. *J. Mammary Gland Biol. Neoplasia.* 11:151–163.
7. Pickup, M. W., H. Laklai, ..., H. L. Moses. 2013. Stromally derived lysyl oxidase promotes metastasis of transforming growth factor- β -deficient mouse mammary carcinomas. *Cancer Res.* 73:5336–5346.
8. Conklin, M. W., J. C. Eickhoff, ..., P. J. Keely. 2011. Aligned collagen is a prognostic signature for survival in human breast carcinoma. *Am. J. Pathol.* 178:1221–1232.

9. Astin, J. W., J. Batson, ..., C. D. Nobes. 2010. Competition amongst Eph receptors regulates contact inhibition of locomotion and invasiveness in prostate cancer cells. *Nat. Cell Biol.* 12:1194–1204.
10. Abercrombie, M. 1970. Contact inhibition in tissue culture. *In Vitro.* 6:128–142.
11. Abercrombie, M., and J. E. Heaysman. 1953. Observations on the social behavior of cells in tissue culture. I. Speed of movement of chick heart fibroblasts in relation to their mutual contacts. *Exp. Cell Res.* 5:111–131.
12. Moore, R., E. Theveneau, ..., R. Mayor. 2013. Par3 controls neural crest migration by promoting microtubule catastrophe during contact inhibition of locomotion. *Development.* 140:4763–4775.
13. Xue, B., K. Krishnamurthy, ..., S. K. Muthuswamy. 2013. Loss of Par3 promotes breast cancer metastasis by compromising cell-cell cohesion. *Nat. Cell Biol.* 15:189–200.
14. Doyle, A. D., F. W. Wang, ..., K. M. Yamada. 2009. One-dimensional topography underlies three-dimensional fibrillar cell migration. *J. Cell Biol.* 184:481–490.
15. Doyle, A. D., M. L. Kutys, ..., K. M. Yamada. 2012. Micro-environmental control of cell migration—myosin IIA is required for efficient migration in fibrillar environments through control of cell adhesion dynamics. *J. Cell Sci.* 125:2244–2256.
16. Kushiro, K., S. Chang, and A. R. Asthagiri. 2010. Reprogramming directional cell motility by tuning micropattern features and cellular signals. *Adv. Mater.* 22:4516–4519.
17. Kim, J. H., and A. R. Asthagiri. 2011. Matrix stiffening sensitizes epithelial cells to EGF and enables the loss of contact inhibition of proliferation. *J. Cell Sci.* 124:1280–1287.
18. Muthuswamy, S. K., D. Li, ..., J. S. Brugge. 2001. ErbB2, but not ErbB1, reinitiates proliferation and induces luminal repopulation in epithelial acini. *Nat. Cell Biol.* 3:785–792.
19. Sommers, C. L. C., E. W. E. Thompson, ..., S. W. S. Byers. 1991. Cell adhesion molecule uvomorulin expression in human breast cancer cell lines: relationship to morphology and invasive capacities. *Cell Growth Differ.* 2:365–372.
20. Oka, H., H. Shiozaki, ..., T. Mori. 1993. Expression of E-cadherin cell adhesion molecules in human breast cancer tissues and its relationship to metastasis. *Cancer Res.* 53:1696–1701.
21. Mbalaviele, G., C. R. Dunstan, ..., T. Yoneda. 1996. E-cadherin expression in human breast cancer cells suppresses the development of osteolytic bone metastases in an experimental metastasis model. *Cancer Res.* 56:4063–4070.
22. Seton-Rogers, S. E., Y. Lu, ..., J. S. Brugge. 2004. Cooperation of the ErbB2 receptor and transforming growth factor beta in induction of migration and invasion in mammary epithelial cells. *Proc. Natl. Acad. Sci. USA.* 101:1257–1262.
23. Carmona-Fontaine, C., H. K. Matthews, ..., R. Mayor. 2008. Contact inhibition of locomotion in vivo controls neural crest directional migration. *Nature.* 456:957–961.
24. Abercrombie, M., and J. E. Heaysman. 1954. Invasiveness of sarcoma cells. *Nature.* 174:697–698.
25. Batson, J., L. Maccarthy-Morrogh, ..., C. D. Nobes. 2014. EphA receptors regulate prostate cancer cell dissemination through Vav2-RhoA mediated cell-cell repulsion. *Biol. Open.* 3:453–462.
26. Cheung, K. J., E. Gabrielson, ..., A. J. Ewald. 2013. Collective invasion in breast cancer requires a conserved basal epithelial program. *Cell.* 155:1639–1651.
27. Levental, K. R., H. Yu, ..., V. M. Weaver. 2009. Matrix cross-linking forces tumor progression by enhancing integrin signaling. *Cell.* 139:891–906.

Biophysical Journal, Volume 110

Supplemental Information

Regulators of Metastasis Modulate the Migratory Response to Cell Contact under Spatial Confinement

Daniel F. Milano, Nicholas A. Ngai, Senthil K. Muthuswamy, and Anand R. Asthagiri

Regulators of metastasis modulate the migratory response to cell contact under spatial confinement

D.F. Milano, N.A. Ngai, S.K. Muthuswamy, and A.R. Asthagiri

Supplemental Material

Cell sliding behavior does not correlate with single-cell migration speed

Reversal of direction upon cell-cell contact is not analogous to the physics of an elastic collision of billiard balls. Inertial effects are negligible in cell migration and cell-cell collision response. With this caveat in mind, it is nevertheless useful to probe whether the sliding response to cell-cell collisions exhibits a correlation with single-cell migration speed. We measured the migration speed of three cell groups: 10A cells (poor sliding), 231 cells (effective sliding) and TGF β -treated 10A cells (effective sliding). While 10A cells are slightly faster (15-20%) than 231 cells, 10A cells are slower than TGF β -treated counterparts (data not shown). Thus, there is no apparent correlation between single-cell migration speed and the ability to slide in response to cell-cell collisions.

Characteristic Fibrillar Dimension (CFD)

Across all cell lines and genetic perturbations investigated in this study, the fraction of collisions that result in a slide ranged from 0% to a maximum of approximately 50% in highly metastatic cells (Fig. S1). The likelihood of contact-initiated sliding increased on wider micropatterns. We sought to quantify the characteristic fibrillar-like dimension (CFD) at which each cell line achieved an intermediate level of sliding, i.e., 25% of collisions result in a slide.

To avoid fitting our data to over-parameterized, complex models, we used a simpler conservative approach to interpolate the CFD value. A linear model was used to describe the dependence of fraction sliding on micropattern width (Fig. S1), and this model was then used to determine the CFD. If the predicted value of the CFD was significantly outside the range of micropattern widths investigated in this work (6-33 μm), it was considered an extrapolation, and we disregard the numerical value of the CFD and report only whether it was below 6 μm or above 33 μm . If the value of the CFD was within the 6-33 μm , we report the interpolated value.

The calculated values for the CFD, the micropattern width at which an intermediate level of sliding is achieved, are shown in Figure 5. The CFD was at or below 10 μm for metastatic MDA-MB-231 and BT549 cells, indicating that highly metastatic cells are able to slide effectively even in narrow fiber-like spatial constraints. On the other hand, the CFD is higher than 33 μm for MCF-10A cells. Reducing E-cadherin expression or perturbing PARD3 in combination with ErbB2 enables intermediate levels of sliding at lower micropattern widths of 23-25 μm than the parental 10A cells. Thus, genetic perturbations that promote metastasis reduce the degree of fibrillar organization needed to achieve cell sliding.

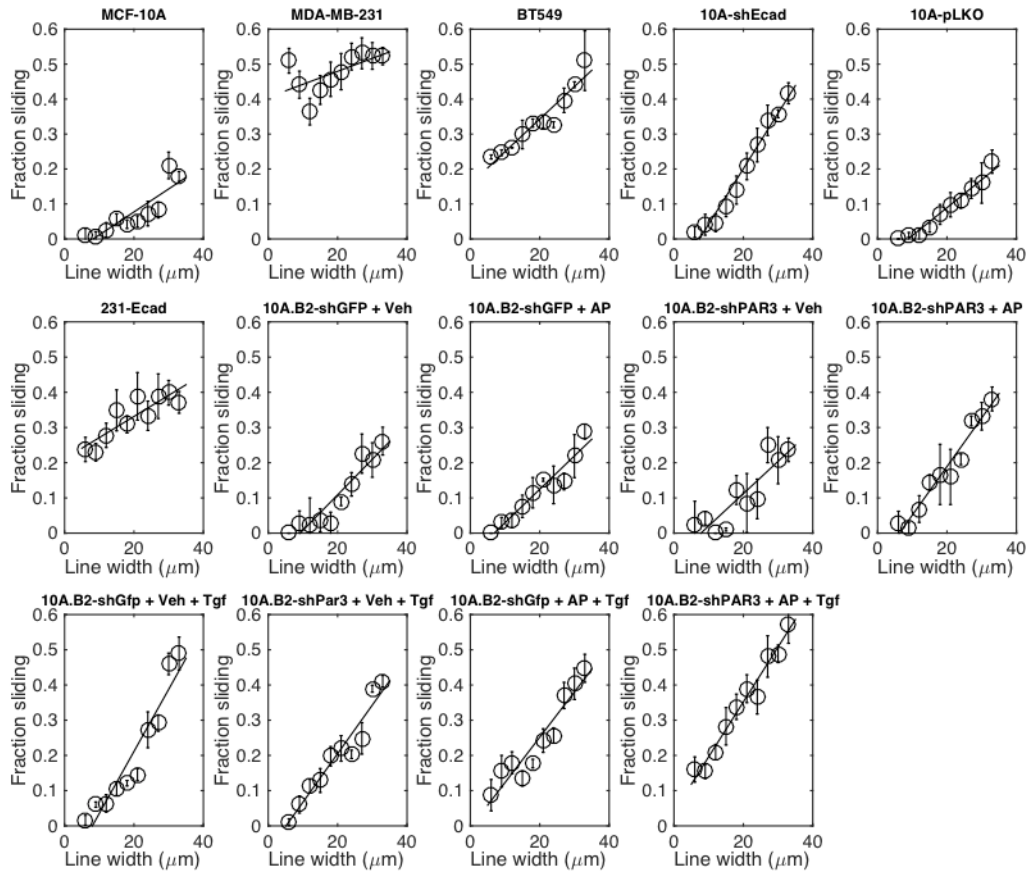


Figure S1. Linear models were used to capture the dependence of fraction sliding on the width of the micropattern for the different cell systems investigated in this work. The value of line width (CFD) at which a moderate efficiency of sliding (fraction sliding = 0.25) was determined for each cell type.

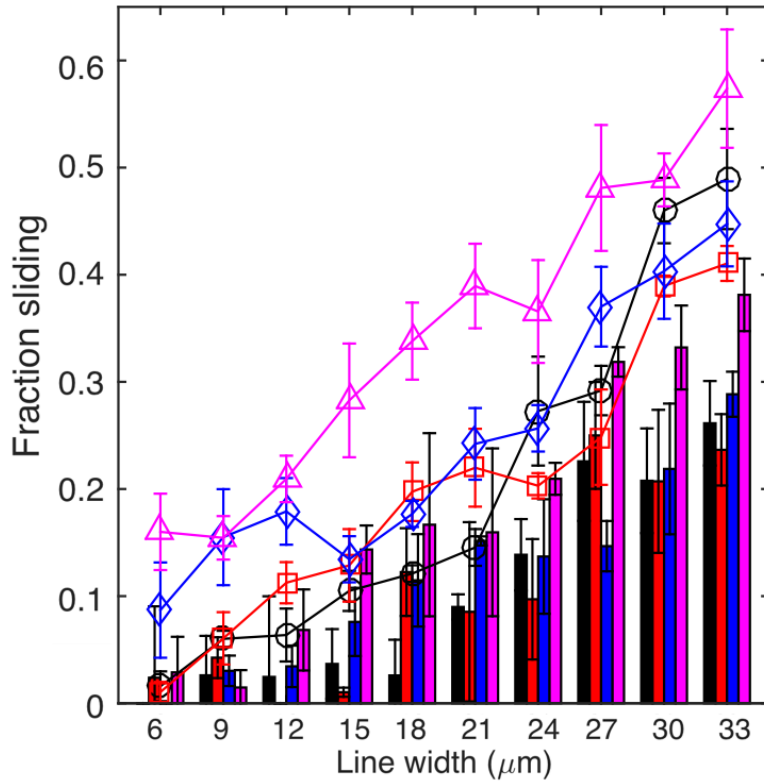


Figure S2. Effect of TGF β treatment on the sliding behavior of 10A.B2 cells that have perturbations in PARD3 and ErbB2 signaling. Bars represent cases without TGF β and are data replotted from Figure 4, and lines in the same color represent the corresponding case treated with 20 ng/mL TGF β . 10A.B2-shGFP and 10A.B2-shPAR3 cells treated with vehicle control (black and red, respectively) or with AP1510 (blue and magenta, respectively).

Movie S1. Contact-initiated reversal between MCF-10A cells on 18-micron wide micropattern. Individual frames are captured at 5-minute intervals.

Movie S2. Contact-initiated sliding between MCF-10A cells on 18-micron wide micropattern. Individual frames are captured at 5-minute intervals.